Atherosclerosis and Matrix Metalloproteinases: Experimental Molecular MR Imaging in Vivo[1]

Vardan Amirbekian, MD
Juan Gilberto S. Aguinaldo, MD
Smbat Amirbekian, BS
Fabien Hyafil, MD
Esad Vucic, MD
Marc Sirol, MD, PhD
David B. Weinreb, MD
Soizic Le Greneur, PhD
Eric Lancelot, PharmD, PhD
Claire Corot, PharmD, PhD
Edward A. Fisher, MD, PhD
Zorina S. Galis, PhD
Zahi A. Fayad, PhD

Purpose: To evaluate the capability of P947, a magnetic resonance (MR) imaging contrast agent that molecularly targets matrix metalloproteinases (MMPs), to aid detection and imaging of MMPs in atherosclerotic lesions in vivo; its specificity compared with that of P1135; expression and distribution of MMPs in atherosclerotic vessels; and in vivo distribution and molecular localization of fluorescent europium (Eu) P947.

Materials and Methods: The Animal Care and Use Committee approved all experiments. P947 was synthesized by attaching a gadolinium chelate (1,4,7,10-tetraazacyclododecane-N,N′,N″,N‴-tetraacetic acid) to a peptide that specifically binds MMPs. Scrambled form of P947 (P1135) was synthesized by replacing the targeting moiety of P947 with a scrambled peptide lacking the ability to bind MMPs. P947, P1135, and gadoterate meglumine were injected into atherosclerotic apolipoprotein E–deficient and wild-type mice. The aortic MR imaging enhancement produced by the contrast agents was measured at different times and was compared by using one-way analysis of variance. MMP expression was investigated in the aortas by using MMP immunostaining and in situ MMP zymography. A fluorescent form of P947 (Eu-P947) was synthesized to compare the in vivo distribution of the contrast agent (Eu-P947) with specific MMP immunofluorescent staining.

Results: MMP-targeted P947 facilitated a 93% increase ($P < .001$) in MR image signal intensity (contrast-to-noise ratio [CNR], 17.7 compared with 7.7; $P < .001$) of atherosclerotic lesions in vivo. Nontargeted P1135 (scrambled P947) provided 33% MR image enhancement (CNR, 10.8), whereas gadoterate meglumine provided 5% (CNR, 6.9). Confocal laser scanning microscopy demonstrated colocalization between fluorescent Eu-P947 and MMPs in atherosclerotic plaques. Eu-P947 was particularly present in the fibrous cap region of plaques.

Conclusion: P947 improved MR imaging for atherosclerosis through MMP-specific targeting. The results were validated and provide support for further assessment of P947 as a potential tool for the identification of unstable atherosclerosis.

Supplemental material:
http://radiology.rsnajnls.org/cgi/content/full/2511080539/DC1

[1] From the Translational and Molecular Imaging Institute, Imaging Science Laboratories, Department of Radiology, Zena and Michael A. Wiener Cardiovascular Institute, Marie-Joseé and Henry R. Kravis Cardiovascular Health Center, and Department of Medicine, Mount Sinai School of Medicine, One Gustave L. Levy Place, Box 1234, New York, NY 10029 (V.A., J.G.S.A., S.A., F.H., E.V., M.S., D.B.W., Z.A.F.); Brigham and Women's Hospital, Harvard Medical School, Boston, Mass (V.A.); Sarnoff Cardiovascular Research Foundation, Great Falls, Va (V.A.); Emory University School of Medicine, Atlanta, Ga (S.A.); Guerbet, Aulnay-sous-Bois, France (S.L.G., E.L., C.C.); New York University School of Medicine, New York, NY (E.A.F.); and Indiana University School of Medicine and Lilly Research Laboratories, Indianapolis, Ind (Z.S.G.). From the 2007 RSNA Annual Meeting. Received March 22, 2008; revision requested June 2; final revision received October 10; accepted October 17; final version accepted November 3. Z.A.F., E.L., C.C., S.L. supported by Guerbet. Supported by the Zena and Michael A. Wiener Cardiovascular Institute; the Marie-Josée and Henry R. Kravis Cardiovascular Health Center; the Department of Radiology, Mount Sinai School of Medicine; and National Science Foundation Major Research Instrumentation grant DBI-9724504. V.A. supported by the Sarnoff Cardiovascular Research Foundation. **Address correspondence to** Z.A.F. (e-mail: *Zahi.Fayad@mssm.edu*).

Despite great advances in cardiovascular medicine, atherosclerosis remains the foremost cause of death in developed industrialized societies (1,2) and has become the leading cause of death globally (3,4). We do not currently possess clinical tools capable of accurately evaluating atherosclerosis directly or at early stages of disease when interventions may have the greatest effect on altering disease progression.

The rapidly evolving field of molecular imaging will ultimately allow us to accurately assess molecular, cellular, and compositional components of atherosclerotic lesions. This information will be clinically vital to identify vulnerable patients (5,6) and facilitate personalized medical management. Molecular magnetic resonance (MR) imaging is especially appealing as a noninvasive modality to evaluate atherosclerosis because it lacks ionizing radiation and possesses the superb spatial resolution necessary to image small-scale pathologic findings such as atherosclerotic lesions (7,8).

Matrix metalloproteinases (MMPs) are implicated in the progression, destabilization, and rupture of atherosclerotic lesions (9–12). Abnormal expression and regulation of MMPs in atherosclerotic plaques may lead to destabilization, resulting in plaque rupture with subsequent thrombosis, occlusion, and detrimental clinical consequences such as myocardial infarction or stroke (13). MMP overexpression has been demonstrated in the vulnerable shoulder regions of human atheroma (9). Macrophage-derived foam cells that are characteristic of unstable plaques have been shown to be major sources of MMPs in human and experimental atherosclerotic lesions (14). Therefore, MMP expression not only is a part of the pathogenesis of atherosclerosis, but it may be predictive of plaque instability (15). Such a potentially pivotal role in the pathogenesis of atherosclerosis suggests that MMPs are a rewarding target for molecular imaging.

Thus, the molecular MR imaging contrast agent that we investigated in this study was P947, which specifically targets MMPs (16,17). P947 is a newer molecular MR imaging agent made of a gadoterate meglumine (Guerbet, Aulnay-sous-Bois, France) moiety covalently bound, by using a linker, to a peptide that specifically binds MMPs at the enzymatic active site (16,18). For the purpose of demonstrating the specificity of P947 for MMPs in vivo, two other contrast agents were used as controls: P1135 (Guerbet), which is an MR imaging analog of P947 for which the peptide sequence has been scrambled, leading to a loss of affinity for MMPs; and P1191 (Guerbet), which is a europium (Eu) derivative of P947 (Eu-P947) with fluorescence emission properties.

The goals of this investigation were as follows: *(a)* to study and validate the in vivo capability of P947 (targeted to MMPs) to assess atherosclerosis in apolipoprotein E (*ApoE*) knockout (*ApoE*-deficient) mice by using MR imaging; *(b)* to evaluate the specificity of P947 for MMPs by comparing its in vivo MR imaging effectiveness to that of P1135 (untargeted, scrambled form of P947 lacking specific binding to MMPs); *(c)* to demonstrate the expression and examine the distribution of MMPs in the atherosclerotic vessels of the mice we used for the in vivo MR imaging experiments; and *(d)* to investigate the in vivo distribution of fluorescent Eu-P947 (also known as P1191) in atherosclerosis and to study the in vivo molecular localization of Eu-P947 in relation to specific MMP fluorescent immunostaining in atherosclerotic lesions (examination of

Advances in Knowledge

- P947 facilitated in vivo MR imaging of atherosclerosis in this experimental investigation.
- The in vivo contrast material–enhanced MR imaging effectiveness of P947 was superior to that of P1135 (untargeted, scrambled form of P947 lacking specific binding to matrix metalloproteinases [MMPs]) and to gadoterate meglumine (a standard gadolinium-based contrast agent).
- Data from this study suggest that P947 specifically targets MMPs in atherosclerosis.
- P947 is in its early stages of development; further investigation is needed to explore its potential as a molecular MR imaging contrast agent.

Implications for Patient Care

- Specific molecular imaging of atherosclerosis will give clinicians the unprecedented ability to detect pathologic findings at early stages before irreversible damage has taken place.
- P947 may facilitate specific noninvasive assessment of atherosclerosis.
- P947 could potentially also be used to evaluate atherosclerotic plaque instability.

Published online before print
10.1148/radiol.2511080539

Radiology 2009; 251:429–438

Abbreviations:
CNR = contrast-to-noise ratio
MMP = matrix metalloproteinase
NER = normalized enhancement ratio
SI = signal intensity
WT = wild type

Author contributions:
Guarantors of integrity of entire study, J.G.S.A., E.L., Z.A.F.; study concepts/study design or data acquisition or data analysis/interpretation, all authors; manuscript drafting or manuscript revision for important intellectual content, all authors; manuscript final version approval, all authors; literature research, V.A., J.G.S.A., S.A., F.H., E.V., M.S., D.B.W., E.L., C.C., Z.S.G., Z.A.F.; clinical studies, V.A., J.G.S.A., M.S., E.L., Z.A.F.; experimental studies, V.A., J.G.S.A., S.A., F.H., E.V., M.S., D.B.W., S.L.G., E.L., C.C., Z.S.G., Z.A.F.; statistical analysis, J.G.S.A., E.V., M.S., Z.A.F.; and manuscript editing, V.A., J.G.S.A., S.A., F.H., E.V., M.S., D.B.W., C.C., Z.S.G., Z.A.F.

Funding:
This research was supported by the National Institutes of Health and the National Heart, Lung, and Blood Institute (grant nos. R01 HL71021, R01 HL78667), the National Institutes of Health (grant nos. U01 HL70524, R01 HL84312, 1 S10 RR09145-01), the National Heart, Lung, and Blood Institute (grant nos. R01 HL64689, R01 HL71061), and the National Institutes of Health and the National Cancer Institute (grant no. 5R24 CA095823-04).

See Materials and Methods for pertinent disclosures.

See also Science to Practice in this issue.

possible colocalization between fluorescent Eu-P947 and specific MMPs). A limited part of this work was presented at the American Heart Association scientific meeting (17), but the images in this article are not the same as those published previously (17).

Materials and Methods

This study was partially funded by Guerbet. All contrast agents were provided by Guerbet. The authors who were not employees of Guerbet (V.A., J.G.S.A., S.A., F.H., E.V., M.S., D.B.W., E.A.F., Z.S.G., Z.A.F.) had full control of the data; those who were employees (S.L.G., E.L., C.C.) did not have control of the data.

Synthesis and Characterization of Contrast Agents

P947 was synthesized by Guerbet through the coupling of an MMP-binding peptide to the gadolinium chelate 1,4,7,10-tetraazacyclododecane-N,N′,N″,N‴-tetraacetic acid, as described in Appendix E1 (*http://radiology.rsnajnls.org/cgi/content/full/2511080539/DC1*). P1135 (Guerbet) was synthesized by using the same steps as were used for P947 except that the peptide that was attached was scrambled in sequence so that the ability to bind MMPs was lost (the molecular weight and size were identical to those of P947). Eu-P947 (fluorescent P947) was synthesized by using the same steps as those for P947 except that europium was used in place of gadolinium in the 1,4,7,10-tetraazacyclododecane-N,N′,N″,N‴-tetraacetic acid moiety. Gadoterate meglumine (Dotarem; Guerbet) is a standard nonspecific gadolinium-based contrast agent that was used as one of the reference compounds.

Animal Protocol

Atherosclerotic *ApoE*-deficient mice (C57BL/6) (Jackson Laboratory, Bar Harbor, Me) and matched normal (nonatherosclerotic) wild-type (WT) mice (Jackson Laboratory) were used in the experiments, as described in Appendix E1 (*http://radiology.rsnajnls.org/cgi/content/full/2511080539/DC1*). The Animal Care and Use Committee for Mount Sinai School of Medicine, New York, NY, approved all experiments.

In Vivo MR Imaging by Using P947 and Various Controls

In vivo MR imaging was performed (19) with a 9.4-T, 89-mm bore MR imaging system operating at a proton frequency of 400 MHz (Bruker Instruments, Billerica, Mass), as described in Appendix E1 (*http://radiology.rsnajnls.org/cgi/content/full/2511080539/DC1*). After preinjection baseline MR imaging, *ApoE*-deficient mice were injected, via a tail-vein injection catheter (MTV no. 06; Strategic Applications, Libertyville, Ill), with either MMP-targeted P947 (n = 16) or the untargeted scrambled control P1135 (n = 5) at 100 μmol of gadolinium per kilogram. For the control group, *ApoE*-deficient mice (n = 6) were injected (at 100 μmol of gadolinium per kilogram) with the standard nonspecific gadolinium-based MR contrast agent gadoterate meglumine. In addition, as another control group, WT mice were injected with equivalent doses of P947 (n = 4). MR imaging was performed at 1, 2, 3, and 22 hours after injection. Slices were precisely anatomically matched (V.A., J.G.S.A., Z.A.F., M.S.) to the sections obtained on the preinjection baseline image (7).

Analysis of MR Imaging Results and Pathologic Correlation

After the 22-hour postinjection image, the animals were sacrificed. The aortas were carefully isolated by using microscopic dissection and were fixed for standard pathologic analysis. The histologic slides from the atherosclerotic aortas were then matched to the MR image sections for comparison and correlation. To quantitatively analyze the MR imaging results, signal intensity (SI) measurements were obtained by using regions of interest on the aortic wall, with four points in four Cartesian quadrants of the aorta on each section, as described in Appendix E1 (*http://radiology.rsnajnls.org/cgi/content/full/2511080539/DC1*). The contrast-to-noise (CNR) ratio of the aortic wall (W) to the lumen (L) ($CNR_{W/L}$) was calculated for each section by using Equation (1):

$$CNR_{W/L} = \frac{[(W_1 + W_2 + W_3 + W_4)/4] - L_{SI}}{\text{SD of Noise}}, \quad (1)$$

where W_n is the SI value of the aortic wall in quadrant n, L_{SI} is the SI of the lumen, and SD is the standard deviation.

For each matched section, the normalized enhancement ratio (NER) and percentage NER were used to measure the normalized SI enhancement of the aortic wall, relative to muscle, after contrast agent injection by using Equations (2) and (3), as follows:

$$NER = \frac{\left[\left(W_{1POST} + W_{2POST} + W_{3POST} + W_{4POST}\right)/4\right]/SI_{MPost}}{\left[\left(W_{1PRE} + W_{2PRE} + W_{3PRE} + W_{4PRE}\right)/4\right]/SI_{MPre}}, \quad (2)$$

$$\text{Percentage NER} = (\text{NER} - 1)\cdot 100, \quad (3)$$

where $W_{n\text{POST}}$ is the SI of the aortic wall in quadrant n after injection of contrast agent, $W_{n\text{PRE}}$ is the SI of the aortic wall in quadrant n before injection of contrast agent, SI_{MPost} is the SI of muscle after contrast agent injection, and SI_{MPre} is the SI of muscle before contrast agent injection.

MMP Immunohistochemical and Pathologic Analysis

Abdominal aortas matching the MR imaging area were removed, sectioned, and stained by using Masson trichrome staining, as described in Appendix E1 (*http://radiology.rsnajnls.org/cgi/content/full/2511080539/DC1*). Immunostaining intended for light microscopy was performed, targeting MMP-2, MMP-3, and MMP-9 by using standard established techniques, as described in Appendix E1 (*http://radiology.rsnajnls.org/cgi/content/full/2511080539/DC1*). In situ gelatin zymography was performed by using standard established techniques, as described in Appendix E1

(*http://radiology.rsnajnls.org/cgi/content/full/2511080539/DC1*), and imaging was performed by using a laser scanning confocal microscope.

Confocal Laser Scanning Fluorescence Microscopy

Abdominal aortas matching the MR imaging area from *ApoE*-deficient mice were fluorescently immunostained for MMP-2, MMP-3, or MMP-9 by using standard established techniques, as described in Appendix E1 (*http://radiology.rsnajnls.org/cgi/content/full/2511080539/DC1*). Confocal laser scanning fluorescence microscopy was performed.

Data and Statistical Analysis

To determine the significance of the SI changes at different times, a paired *t* test analysis was performed by using the NER or percentage NER from matched sections in the same animals at different times. A one-way analysis of variance, with Bonferroni post hoc multiple comparison tests, was used to compare the NER or percentage NER values among P947-injected, P1135-injected, and gadoterate meglumine–injected *ApoE*-deficient mouse groups, as well as the P947-injected WT mouse group. For all statistical analyses, *P* values less than .05 were considered significant. The analysis was performed by using software (Number Crunching Statistical System, 2001; NCSS, Kaysville, Utah).

Results

P947 MR Imaging for in Vivo Atherosclerotic Lesions

Prior to injection of the contrast agent, MR imaging was performed in all mice at baseline. Before injection of the contrast agent, MR imaging of *ApoE*-deficient mice showed a heterogeneous distribution of aortic wall thickening. Aortic wall thickening correlates strongly with the presence of atherosclerotic lesions, a finding that is consistent with results in our previously published studies (7). As anticipated, baseline MR imaging of WT mice showed no regions of aortic wall thickening.

After injection of P947, designed to specifically target MMPs, we (V.A., J.G.S.A., Z.A.F., M.S., S.A., F.H.) observed very strong and significant heterogeneous enhancement of the aortic wall in *ApoE*-deficient mice (Fig 1a). The change in the MR image SI of the aorta was measured by using the NER and percentage NER. In particular, by using *ApoE*-deficient mice, at 1 hour after injection, P947 provided an average

Figure 1

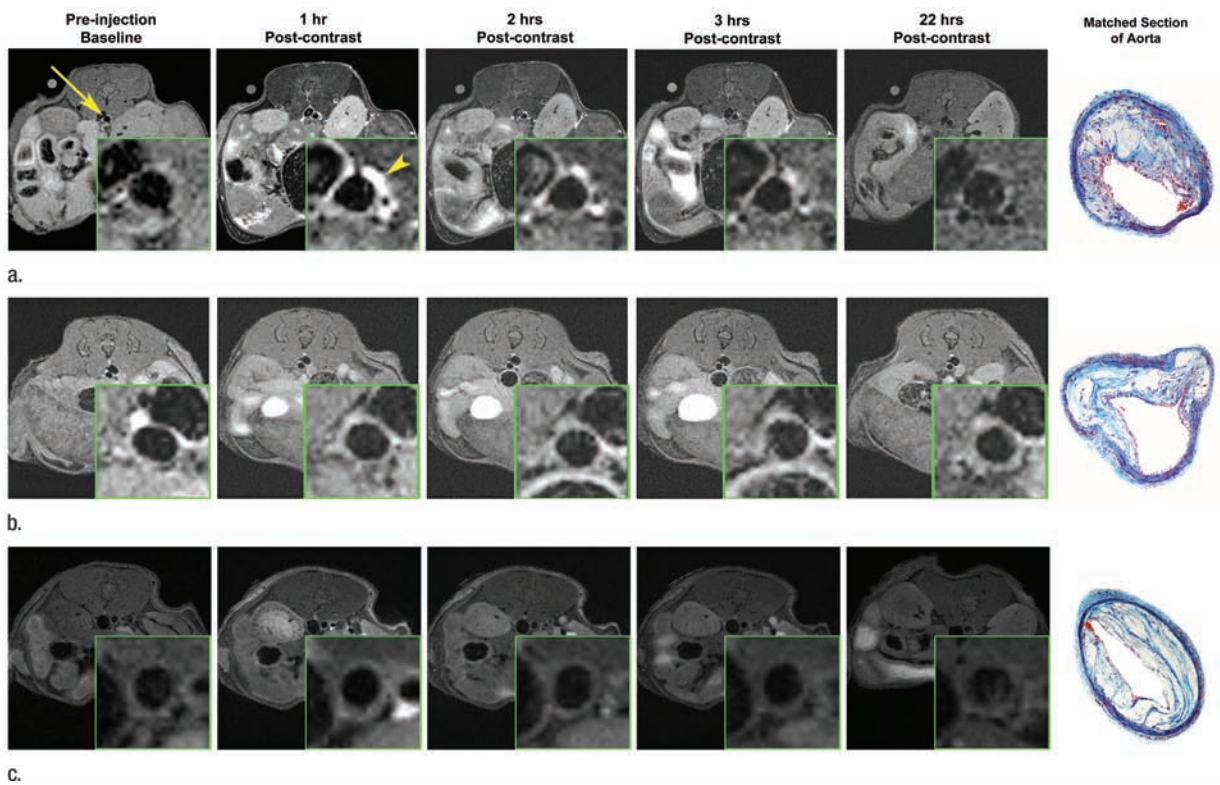

Figure 1: In vivo MR images acquired in atherosclerotic *ApoE*-deficient mice. **(a)** At baseline (before injection) and up to 22 hours after injection of MMP-targeted P947. **(b)** With untargeted P1135 (scrambled form of P947). **(c)** With standard nontargeted gadoterate meglumine. Insets are enlargements of aorta (arrow). Arrowhead points to MR inset of atherosclerotic aorta after injection with P947. **(a–c)** Farthest right images show hematoxylin-eosin–stained sections of aorta at identical anatomic level as MR images from same animal (17).

Radiology

Figure 2

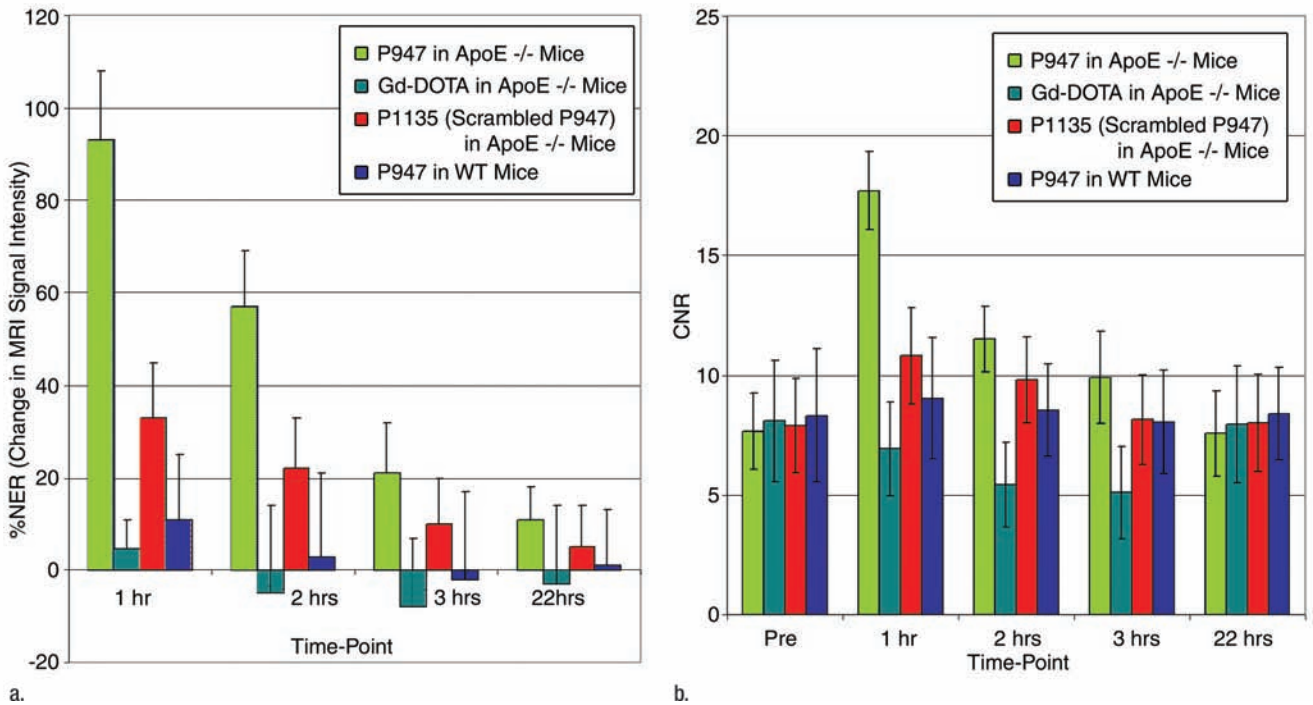

Figure 2: Graphs depict quantitative temporal MR imaging results. In vivo MR image SI of aortic wall at different times measured with **(a)** percentage NER and **(b)** CNR in *ApoE*-deficient mice injected with MMP-targeted P947, gadoterate meglumine *(Gd-DOTA)*, and untargeted P1135 and in WT mice injected with P947. In *ApoE*-deficient mice at 1 hour after injection, MMP-targeted P947 showed CNR of 17.7 (percentage NER, 93%); with gadoterate meglumine, CNR was 6.9 (percentage NER, 5%), with untargeted P1135, CNR was 10.8 (percentage NER, 33%), and in WT mice injected with P947, CNR was 8.3 (percentage NER, 11%).

aortic MR image signal enhancement of 127% (percentage NER), corresponding to a mean NER of 2.27 ± 0.15 (standard deviation) when standardized to an externally placed standard solution of gadolinium and percentage NER of 93% (mean NER, 1.93 ± 0.15), when standardized to adjacent muscle tissue, as shown in Figures 1 and 2. In comparison, the percentage NER was 33% (mean NER, 1.33 ± 0.12) when we used P1135 and 4.6% (mean NER, 1.05 ± 0.06) with gadoterate meglumine (both also standardized to muscle). As demonstrated in Figures 1 and 2, these results translate into a threefold increase in the MR image SI in the atherosclerotic aortic wall when we used P947 compared with P1135, a permuted derivative of P947 with the amino acid sequence scrambled such that specific binding to MMPs is lost, supporting an MMP-specific image enhancement mechanism. In addition, the SI increase with P947 was 15-fold higher when compared with the standard nonspecific gadolinium-based MR imaging contrast agent gadoterate meglumine ($P < .001$) (Fig 2).

In nonatherosclerotic WT mice, at 1 hour after injection, P947 provided minimal change of the average aortic MR imaging SI that was homogeneous in nature and was not significant from baseline (Fig 2). At 2 and 3 hours after injection, no significant changes were seen ($P > .05$) of the aortic MR image SI values in WT mice (Fig 2).

Expression and Activity of MMPs in Mice at MR Imaging

After the MR imaging experiments were completed, the mice were sacrificed for various types of pathologic analyses of the atherosclerotic aortas (all animals). Pathologic analysis of aortic tissue sections was performed to validate expression of MMPs in atherosclerotic plaques in *ApoE*-deficient mice used for the MR imaging experiments in this study. Tissue sections prepared from *ApoE*-deficient mouse aortas were immunostained for MMP-2, MMP-3, and MMP-9 for immunohistopathologic analysis. Atherosclerotic sections of *ApoE*-deficient mouse aortas revealed intense MMP-3 staining, as shown in Figure 3, consistent with substantial expression of MMP-3. Aortic sections immunostained for MMP-9 also showed high-level staining (Fig 3) that indicates a substantial level of MMP-9 in atherosclerotic lesions of *ApoE*-deficient mice. Finally, MMP-2–immunostained sections were also obtained (Fig 3) but showed less robust staining as compared with that for sections immunostained with MMP-3 and MMP-9.

To further assess MMPs in atherosclerosis, we performed (F.H., E.V., J.G.S.A., V.A., D.B.W.) in situ MMP zymography on atherosclerotic aortic

Radiology

Figure 3

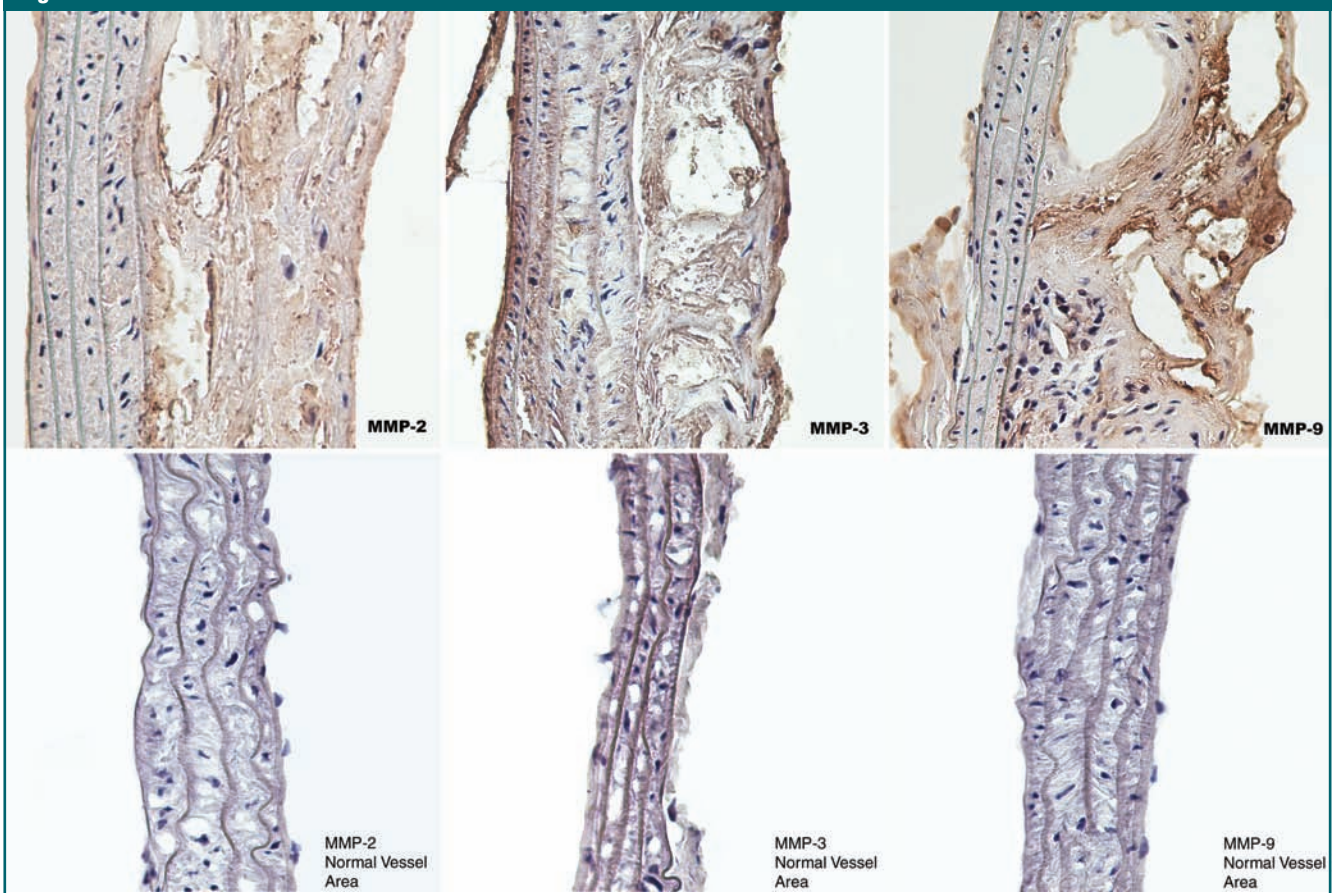

Figure 3: Light microscopic images show specific MMP immunostaining of atherosclerotic aortic lesions from *ApoE*-deficient mice. Top: Increased expression of MMP-2, MMP-3, and MMP-9. Bottom: Normal vessel areas. Sections were taken from aortas of mice used in in vivo MR imaging experiments.

Figure 4

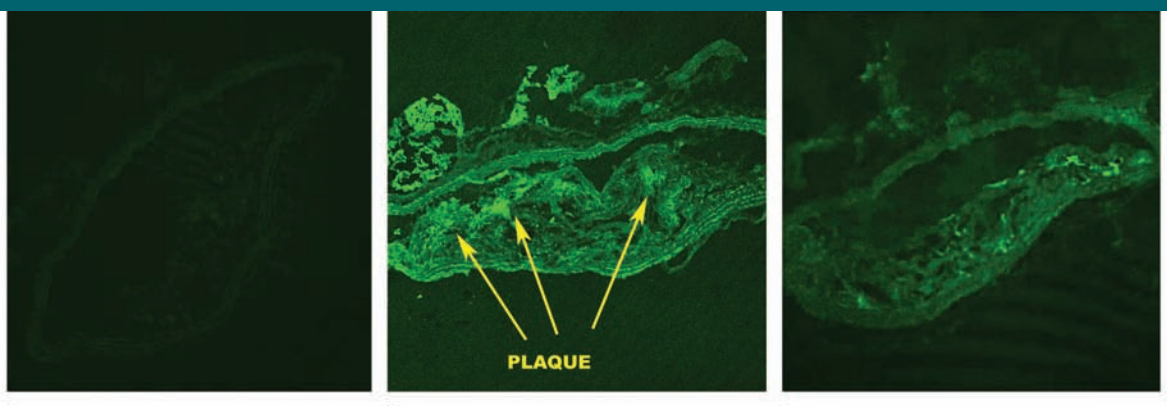

Figure 4: Fluorescence microscopic images from MMP in situ zymography of mouse aortas demonstrate increased MMP gelatinolytic activity in atherosclerotic sections. **(a)** Control section that was incubated with gel alone shows that there is negligible intrinsic fluorescence. **(b)** Atherosclerotic aortic section incubated with gel and dye that fluoresced only after cleavage by MMPs (arrows point to atherosclerotic plaque). **(c)** Atherosclerotic section that was incubated with gel, dye, and ethylenediaminetetraacetic acid, which blocks MMP activity, demonstrates that most of fluorescence seen on **b** was caused by active MMP cleavage of dye. All sections taken from mice used in in vivo MR imaging experiments.

sections from *ApoE*-deficient mice that were used in the imaging experiments. In contrast to MMP immunohistostaining, which is used to assess expression of both active and inactive MMPs, the information gathered by using MMP zymography represents MMP enzymatic activity. To perform the in situ zymography, we used an MMP substrate that becomes fluorescent only after cleavage by active MMPs. The in situ MMP zymography revealed substantial MMP activity in the aortic atherosclerotic lesions, as shown in Figure 4b. After broad-spectrum blockage of MMP activity by using ethylenediaminetetraacetic acid, there was a large decrease in the fluorescent activity seen in the atherosclerotic sections (Fig 4c). This behavior indicates that most of the fluorescence seen during MMP zymography is caused by MMP enzymatic activity. Sections incubated as controls did not show fluorescence (Fig 4a).

Distribution of Fluorescent P947 in Atherosclerotic Sections and Colocalization with MMPs

To confirm the in vivo distribution and localization of P947, we (E.L., C.C., S.L.G.) synthesized Eu-P947, replacing gadolinium on a one-to-one basis with europium (a lanthanide that is chemically similar to gadolinium), which fluoresces when excited at the appropriate wavelength, allowing detection by using confocal laser scanning microscopy. After intravenous injection of Eu-P947 (fluorescent P947), *ApoE*-deficient mice were sacrificed, and the aortas were dissected out to prepare tissue sections. The atherosclerotic aortic sections were then imaged by using confocal laser scanning fluorescence microscopy. The images obtained showed that Eu-P947 localized within areas of aortic plaque, as shown in Figure 5a. Most notably, in sections where a fibrous cap was apparent, there was significant Eu-P947 fluorescence signal emanating from the fibrous cap (far left and left images of Fig 5a).

To investigate the distribution of Eu-P947 in relation to MMPs, we (D.B.W., J.G.S.A., S.A., V.A.) performed specific fluorescent MMP immunostaining of aortic sections from *ApoE*-deficient mice previously injected with Eu-P947. Specifically, we performed fluorescent immunostaining for MMP-2, MMP-3, and MMP-9 at 1 hour after injection (when the MR image signal was maximal with P947). Confocal laser scanning microscopy revealed substantial overlap in the distribution of MMP-3 fluorescence and Eu-P947 fluorescence, as shown in Figure 5c (combined overlaid image, right). Similarly, coregistration was present between the fluorescent signal emitted by Eu-P947 and MMP-9, as well as by MMP-2 (Fig 5d and 5b, respectively). Overall, the results of the confocal microscopy indicate that there is colocalization between fluorescent P947 (Eu-P947) and MMPs.

Discussion

A major result of this investigation was that MMP-targeted P947 facilitated significant MR image enhancement (increase of 93%) of the atherosclerotic vessel wall of *ApoE*-deficient mice in vivo. Our findings were specific because nontargeted P1135 (the scrambled form of P947 that has no specific binding to MMPs) delivered only one-third of the enhancement (33%) of P947, whereas gadoterate meglumine (a clinically available nonspecific MR imaging contrast agent) alone enhanced atherosclerotic lesions by only 4.6%, about 1/15 that of P947. These results suggest that the bulk of atherosclerosis enhancement seen with P947 is caused by specific binding, accumulation, or retention of P947, making P947 substantially better than any of the MR imaging contrast agents that we tested in this study.

The MR imaging results of this study correlated well with the standard pathologic findings in the regions of vessels that we imaged. As compared with normal vessels and controls, the atherosclerotic vessels from *ApoE*-deficient mice used in the MR imaging experiments showed significant overexpression of MMP-2, MMP-3, and MMP-9. This finding is consistent with findings in previously published data (9,20–23) and supports our hypothesis that MMP expression is largely responsible for P947-mediated MR imaging enhancement of atherosclerosis in *ApoE*-deficient mice. As an additional mode of validation, in situ MMP zymography was performed on sections of atherosclerotic aortas from the mice used in the experiments. As compared with MMP immunostaining, zymography is a qualitative approach to examining functional MMP activity. The atherosclerotic vessel lesions that we examined showed substantial functional MMP activity. Control sections did not show significant fluorescence. Moreover, sections that were first incubated with a broad-spectrum MMP inhibitor showed dramatically less fluorescence. This indicates that the bulk of fluorescence seen at in situ zymography was caused by functional MMP activity.

The results of confocal laser scanning microscopy strongly suggest colocalization between specific MMPs and fluorescently tagged P947 (Eu-P947). There appeared to be large regions of strong MMP-3 staining that significantly overlapped with Eu-P947 distribution. Similarly, there was good overlap between the distributions of Eu-P947 and MMP-2, as well as MMP-9, which is thought to play a highly detrimental pathogenic role in atherosclerosis of *ApoE*-deficient mice (23). Overall, there were large areas of coregistration between the distribution of specific MMPs and fluorescent Eu-P947. This colocalization further supports the hypothesis that P947 accumulates and gets retained in atherosclerotic plaques largely because of binding by MMPs. We also examined the distribution of fluorescent Eu-P947 alone in atherosclerotic plaques. Notably, in atherosclerotic plaques where a fibrous cap was apparent, we noticed substantial Eu-P947 fluorescent signal by using confocal laser scanning microscopy. MMPs have been previously implicated in atherosclerotic fibrous cap thinning and degradation (9,20–22,24), a process thought to lead to plaque rupture and thrombosis.

The work presented in this study represents an innovative approach to imaging MMPs by using positive (increasing SI)–contrast agent molecular

Figure 5

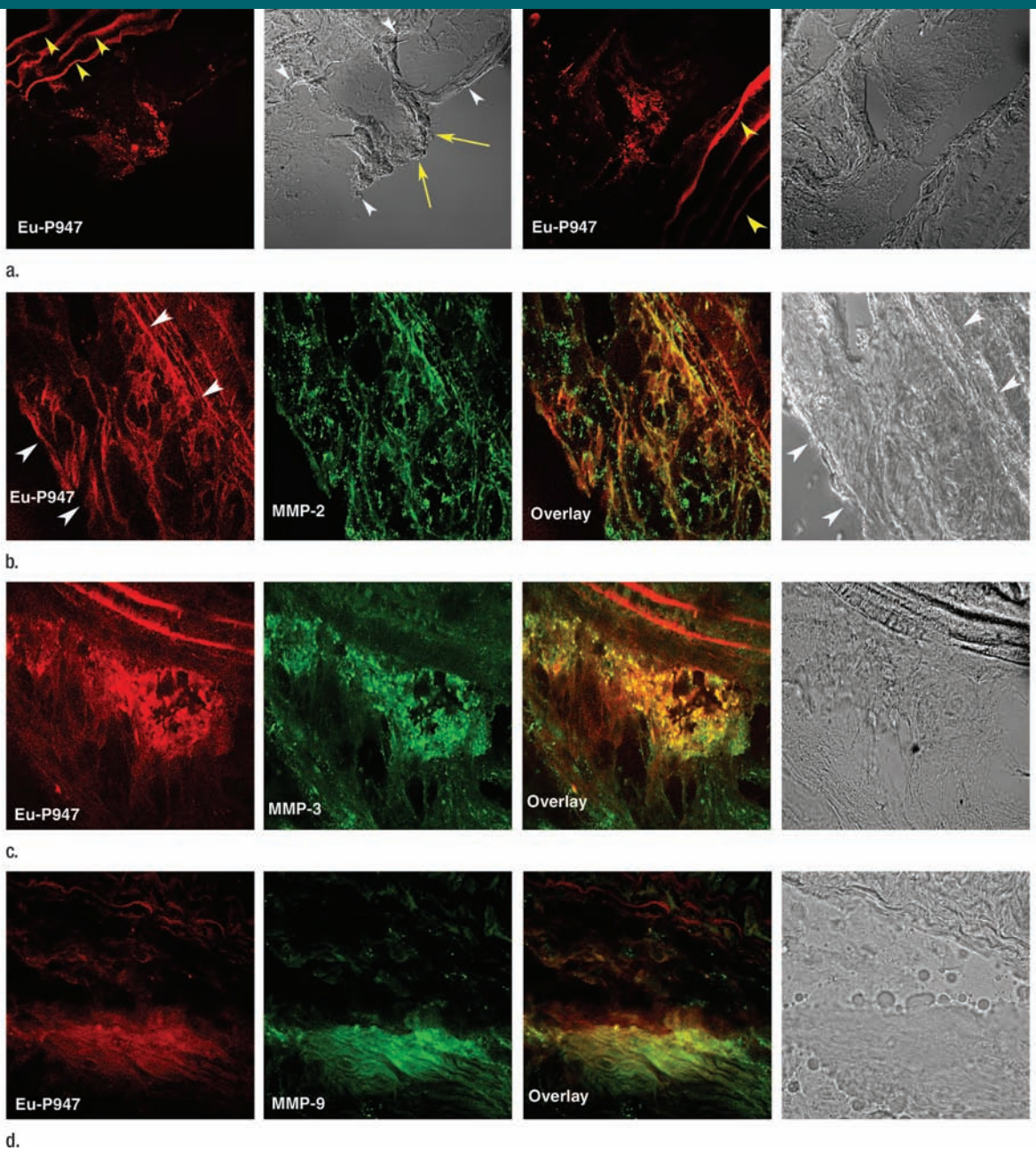

Figure 5: Confocal laser scanning fluorescence microscopic images show Eu-P947 localization alone and colocalization with MMPs. Aortic sections from *ApoE*-deficient mice injected in vivo with Eu-P947 show localization of fluorescent Eu-P947 (red) in atherosclerotic plaques (far left and right images on **a**), alternating with their corresponding differential interference contrast light microscopic images (left and far right images on **a**). Yellow arrowheads indicate elastic lamina. Arrows point to fibrous cap in light microscopic image and show possible accumulation of P947 in fibrous cap (far left image on **a**). Fluorescent immunostaining for MMP-2, MMP-3, and MMP-9 (green on **b–d**, respectively) in aortic sections obtained from *ApoE*-deficient mice injected with fluorescent Eu-P947 (red on **b–d**). Overlaid images at right on **b**, **c**, and **d** show substantial overlap (yellow areas) between Eu-P947 and MMP-2, MMP-3, and MMP-9, respectively. On **b** and **c,** differential interference contrast light microscopic images at right are of respective sections at left. White arrowheads indicate general borders of atherosclerotic plaques on **a** and **b**.

MR imaging. In previous work, researchers attempted to image MMPs with nuclear imaging, including positron emission tomography (PET) (25,26). Researchers used scintigraphy with a radiolabeled broad-spectrum MMP inhibitor to assess MMPs (26). In that study, the issue of the inherent low resolution of scintigraphy was circumvented by inducing a highly localized MMP and foam cell–rich lesion by using carotid artery ligation in *ApoE*-deficient mice fed a high-cholesterol diet (27); however, native atherosclerosis was not imaged in vivo. In vivo imaging of native atherosclerosis by using scintigraphy in mice or in human coronary arteries has yet to be demonstrated. However, nuclear imaging (including PET and single photon emission computed tomography [SPECT]) by using targeted radiotracers will likely offer superb sensitivity because of the very high signal-to-noise ratios possible with radiotracers.

In comparison, MR imaging offers superb anatomic resolution that is orders of magnitude higher than that of scintigraphy, including PET or SPECT. Molecular MR imaging, such as P947-enhanced MR imaging, will offer molecular information combined with superior anatomic resolution, which is vital for imaging small-scale pathologic findings such as atherosclerosis. Optical techniques have also been used to image MMPs. One group imaged gelatinases and MMPs by using a near-infrared fluorescence probe (28), whereas another group used optical techniques to image cathepsin K (a protease with some functions similar to those of MMPs) activity in atherosclerosis (29). Optical techniques offer good sensitivity and, with the use of near-infrared fluorescence probes, the specificity is also quite high, but direct translation of optical techniques into applications in humans remains technically unrealized for now.

At this time, it is not possible to use optical techniques to image structures that are deeper than a couple of centimeters beyond the surface. As such, application for noninvasive imaging in patients is currently not possible. Molecular MR imaging of atherosclerosis has been investigated by using targeted imaging of neovascularization through the molecular target $\alpha_v\beta_3$ integrin (30), whereas others have targeted adhesion molecules, including vascular adhesion molecule 1 (31). To evaluate atherosclerosis with MR imaging, we used both gadolinium-carrying micelles (32,33) and molecularly targeted gadolinium immunomicelles to image macrophages through the macrophage scavenger receptor (19). An interesting observation made by Deguchi et al (28) was that there was an absence of MMP activity in atherosclerotic areas without a high content of macrophages (the presence of MMPs seemed to be a surrogate marker for the presence of macrophages). As such, molecular imaging of MMPs may offer a way to indirectly assess plaque macrophage content and macrophage activity. Although in our investigation we did not find gadoterate meglumine to be very helpful for imaging atherosclerosis, researchers have used gadopentetate dimeglumine to image fibrous components of atherosclerotic plaques with intravascular MR imaging, a relatively invasive imaging approach (34).

There were limitations to this study. P947 is a newer contrast agent, and we currently do not have substantial data regarding potential toxicity of this agent, including data in regard to tissue retention of gadolinium and nephrogenic systemic fibrosis. The goals of this study did not and could not realistically include full characterization of toxic effects, pharmacokinetics, and pharmacodynamics of this agent. These topics will require careful future investigation in multiple staged studies. Another potential limitation is translation to MR imaging for atherosclerosis in humans. Although it is entirely possible to perform excellent MR imaging of carotid artery and aortic atherosclerosis in patients, technical barriers still remain that make adequate MR imaging of the coronary arteries difficult.

In summary, we showed that P947 targeted to MMPs facilitated specific in vivo assessment of atherosclerosis at a molecular pathologic level. Knowledge about MMP content and activity may aid in the prediction of the vulnerability of plaque to rupture and thrombosis. Therefore, with proper development and investigation, imaging with P947 (or similar MMP imaging approaches) may contribute substantially to preclinical and clinical evaluation of atherosclerosis.

Acknowledgments: We thank the Lang Center for Research, the New York Hospital of Queens affiliate of Weill Cornell Medical College of Cornell University, for research elective time and the MSSM-Microscopy Shared Resource Facility for performance of confocal laser scanning microscopy.

References

1. Fuster V, Moreno PR, Fayad ZA, Corti R, Badimon JJ. Atherothrombosis and high-risk plaque. I. Evolving concepts. J Am Coll Cardiol 2005;46:937–954.
2. Heart disease and stroke statistics—2006 update. American Heart Association Web site. http://www.americanheart.org/downloadable/heart/1136308648540Statupdate2006.pdf. Published 2006. Accessed September 23, 2006.
3. Tunstall-Pedoe H. Preventing chronic diseases: a vital investment. WHO Global report. Geneva, Switzerland: World Health Organization, 2005. *http://www.who.int/chp/chronic_disease_report/contents/part1.pdf.* Accessed January 6, 2008.
4. Anderson GF, Chu E. Expanding priorities: confronting chronic disease in countries with low income. N Engl J Med 2007;356:209–211.
5. Naghavi M, Libby P, Falk E, et al. From vulnerable plaque to vulnerable patient: a call for new definitions and risk assessment strategies. II. Circulation 2003;108:1772–1778.
6. Naghavi M, Libby P, Falk E, et al. From vulnerable plaque to vulnerable patient: a call for new definitions and risk assessment strategies. I. Circulation 2003;108:1664–1672.
7. Fayad ZA, Fallon JT, Shinnar M, et al. Noninvasive in vivo high-resolution magnetic resonance imaging of atherosclerotic lesions in genetically engineered mice. Circulation 1998;98:1541–1547.
8. Fayad ZA, Fuster V. Clinical imaging of the high-risk or vulnerable atherosclerotic plaque. Circ Res 2001;89:305–316.
9. Galis ZS, Sukhova GK, Lark MW, Libby P. Increased expression of matrix metalloproteinases and matrix degrading activity in vul-

nerable regions of human atherosclerotic plaques. J Clin Invest 1994;94:2493–2503.

10. Sukhova GK, Schonbeck U, Rabkin E, et al. Evidence for increased collagenolysis by interstitial collagenases-1 and -3 in vulnerable human atheromatous plaques. Circulation 1999;99:2503–2509.
11. Dollery CM, Owen CA, Sukhova GK, Krettek A, Shapiro SD, Libby P. Neutrophil elastase in human atherosclerotic plaques: production by macrophages. Circulation 2003;107:2829–2836.
12. Loftus IM, Naylor AR, Goodall S, et al. Increased matrix metalloproteinase-9 activity in unstable carotid plaques: a potential role in acute plaque disruption. Stroke 2000;31:40–47.
13. Galis ZS, Khatri JJ. Matrix metalloproteinases in vascular remodeling and atherogenesis: the good, the bad, and the ugly. Circ Res 2002;90:251–262.
14. Galis ZS, Sukhova GK, Kranzhofer R, Clark S, Libby P. Macrophage foam cells from experimental atheroma constitutively produce matrix-degrading proteinases. Proc Natl Acad Sci U S A 1995;92:402–406.
15. Galis ZS. Vulnerable plaque: the devil is in the details. Circulation 2004;110:244–246.
16. Lancelot E, Amirbekian V, Brigger I, et al. Evaluation of matrix metalloproteinases in atherosclerosis using a novel noninvasive imaging approach. Arterioscler Thromb Vasc Biol 2008;28:425–432.
17. Amirbekian S, Aguinaldo JG, Amirbekian V, et al. Abstract 1459: using P947 for specifically targeted molecular MRI of matrix metalloproteinases in atherosclerosis and colocalization of fluorescent Eu-P947 within atherosclerotic plaques [abstr]. Circulation 2006;114:II_280.
18. Odake S, Morita Y, Morikawa T, Yoshida N, Hori H, Nagai Y. Inhibition of matrix metalloproteinases by peptidyl hydroxamic acids. Biochem Biophys Res Commun 1994;199:1442–1446.
19. Amirbekian V, Lipinski MJ, Briley-Saebo KC, et al. Detecting and assessing macrophages in vivo to evaluate atherosclerosis noninvasively using molecular MRI. Proc Natl Acad Sci U S A 2007;104:961–966.
20. Henney AM, Wakeley PR, Davies MJ, et al. Localization of stromelysin gene expression in atherosclerotic plaques by in situ hybridization. Proc Natl Acad Sci U S A 1991;88:8154–8158.
21. Halpert I, Sires UI, Roby JD, et al. Matrilysin is expressed by lipid-laden macrophages at sites of potential rupture in atherosclerotic lesions and localizes to areas of versican deposition, a proteoglycan substrate for the enzyme. Proc Natl Acad Sci U S A 1996;93:9748–9753.
22. Johnson JL, Jackson CL, Angelini GD, George SJ. Activation of matrix-degrading metalloproteinases by mast cell proteases in atherosclerotic plaques. Arterioscler Thromb Vasc Biol 1998;18:1707–1715.
23. Johnson JL, George SJ, Newby AC, Jackson CL. Divergent effects of matrix metalloproteinases 3, 7, 9, and 12 on atherosclerotic plaque stability in mouse brachiocephalic arteries. Proc Natl Acad Sci U S A 2005;102:15575–15580.
24. Shah PK, Falk E, Badimon JJ, et al. Human monocyte-derived macrophages induce collagen breakdown in fibrous caps of atherosclerotic plaques: potential role of matrix-degrading metalloproteinases and implications for plaque rupture. Circulation 1995;92:1565–1569.
25. Wagner S, Breyholz HJ, Faust A, et al. Molecular imaging of matrix metalloproteinases in vivo using small molecule inhibitors for SPECT and PET. Curr Med Chem 2006;13:2819–2838.
26. Schäfers M, Riemann B, Kopka K, et al. Scintigraphic imaging of matrix metalloproteinase activity in the arterial wall in vivo. Circulation 2004;109:2554–2559.
27. Ivan E, Khatri JJ, Johnson C, et al. Expansive arterial remodeling is associated with increased neointimal macrophage foam cell content: the murine model of macrophage-rich carotid artery lesions. Circulation 2002;105:2686–2691.
28. Deguchi JO, Aikawa M, Tung CH, et al. Inflammation in atherosclerosis: visualizing matrix metalloproteinase action in macrophages in vivo. Circulation 2006;114:55–62.
29. Jaffer FA, Kim DE, Quinti L, et al. Optical visualization of cathepsin K activity in atherosclerosis with a novel, protease-activatable fluorescence sensor. Circulation 2007;115:2292–2298.
30. Winter PM, Morawski AM, Caruthers SD, et al. Molecular imaging of angiogenesis in early-stage atherosclerosis with alpha (v)beta3-integrin-targeted nanoparticles. Circulation 2003;108:2270–2274.
31. Kelly KA, Allport JR, Tsourkas A, Shinde-Patil VR, Josephson L, Weissleder R. Detection of vascular adhesion molecule-1 expression using a novel multimodal nanoparticle. Circ Res 2005;96:327–336.
32. Lipinski MJ, Amirbekian V, Frias JC, et al. MRI to detect atherosclerosis with gadolinium-containing immunomicelles targeting the macrophage scavenger receptor. Magn Reson Med 2006;56:601–610.
33. Briley-Saebo KC, Amirbekian V, Mani V, et al. Gadolinium mixed-micelles: effect of the amphiphile on in vitro and in vivo efficacy in apolipoprotein E knockout mouse models of atherosclerosis. Magn Reson Med 2006;56:1336–1346.
34. Larose E, Kinlay S, Selwyn AP, et al. Improved characterization of atherosclerotic plaques by gadolinium contrast during intravascular magnetic resonance imaging of human arteries. Atherosclerosis 2008;196:919–925.

Radiology 2009

This is your reprint order form or pro forma invoice

(Please keep a copy of this document for your records.)

Reprint order forms and purchase orders or prepayments must be received 72 hours after receipt of form either by mail or by fax at 410-820-9765. It is the policy of Cadmus Reprints to issue one invoice per order. **Please print clearly**.

Author Name _____
Title of Article _____
Issue of Journal_____ Reprint # _____ Publication Date _____
Number of Pages_____ KB # _____ Symbol Radiology
Color in Article? Yes / No (Please Circle)

Please include the journal name and reprint number or manuscript number on your purchase order or other correspondence.

Order and Shipping Information

Reprint Costs **(Please see page 2 of 2 for reprint costs/fees.)**

_____ Number of reprints ordered $_____
_____ Number of color reprints ordered $_____
_____ Number of covers ordered $_____
Subtotal $_____
Taxes $_____

(*Add appropriate sales tax for Virginia, Maryland, Pennsylvania, and the District of Columbia or Canadian GST to the reprints if your order is to be shipped to these locations*.)

First address included, add $32 for each additional shipping address $_____

TOTAL $_____

Shipping Address **(cannot ship to a P.O. Box) Please Print Clearly**

Name _____
Institution _____
Street _____
City _____ State _____ Zip _____
Country _____
Quantity_____ Fax _____
Phone: Day _____ Evening _____
E-mail Address _____

Additional Shipping Address* **(cannot ship to a P.O. Box)**

Name _____
Institution _____
Street _____
City _____ State _____ Zip _____
Country _____
Quantity _____ Fax _____
Phone: Day _____ Evening _____
E-mail Address _____

** Add $32 for each additional shipping address*

Payment and Credit Card Details

Enclosed: Personal Check _____
Credit Card Payment Details _____

Checks must be paid in U.S. dollars and drawn on a U.S. Bank.

Credit Card: __ VISA __ Am. Exp. __ MasterCard
Card Number _____
Expiration Date_____
Signature: _____

Please send your order form and prepayment made payable to:

Cadmus Reprints
P.O. Box 751903
Charlotte, NC 28275-1903

Note: Do not send express packages to this location, PO Box.

FEIN #:541274108

Invoice or Credit Card Information

Invoice Address **Please Print Clearly**

Please complete Invoice address as it appears on credit card statement

Name _____
Institution _____
Department _____
Street _____
City _____ State _____ Zip _____
Country _____
Phone _____ Fax _____
E-mail Address _____

Cadmus will process credit cards and *Cadmus Journal Services* will appear on the credit card statement.

If you don't mail your order form, you may fax it to 410-820-9765 with your credit card information.

Signature _____ Date _____

Signature is required. By signing this form, the author agrees to accept the responsibility for the payment of reprints and/or all charges described in this document.

RB-1/01/09

Radiology 2009

Black and White Reprint Prices

Domestic (USA only)						
# of Pages	50	100	200	300	400	500
1-4	$239	$260	$285	$303	$323	$340
5-8	$379	$420	$455	$491	$534	$572
9-12	$507	$560	$651	$684	$748	$814
13-16	$627	$698	$784	$868	$954	$1,038
17-20	$755	$845	$947	$1,064	$1,166	$1,272
21-24	$878	$985	$1,115	$1,250	$1,377	$1,518
25-28	$1,003	$1,136	$1,294	$1,446	$1,607	$1,757
29-32	$1,128	$1,281	$1,459	$1,632	$1,819	$2,002
Covers	$149	$164	$219	$275	$335	$393

International (includes Canada and Mexico)						
# of Pages	50	100	200	300	400	500
1-4	$299	$314	$367	$429	$484	$546
5-8	$470	$502	$616	$722	$838	$949
9-12	$637	$687	$852	$1,031	$1,190	$1,369
13-16	$794	$861	$1,088	$1,313	$1,540	$1,765
17-20	$963	$1,051	$1,324	$1,619	$1,892	$2,168
21-24	$1,114	$1,222	$1,560	$1,906	$2,244	$2,588
25-28	$1,287	$1,412	$1,801	$2,198	$2,607	$2,998
29-32	$1,441	$1,586	$2,045	$2,499	$2,959	$3,418
Covers	$211	$224	$324	$444	$558	$672

Color Reprint Prices

Domestic (USA only)						
# of Pages	50	100	200	300	400	500
1-4	$247	$267	$385	$515	$650	$780
5-8	$297	$435	$655	$923	$1194	$1467
9-12	$445	$563	$926	$1,339	$1,748	$2,162
13-16	$587	$710	$1,201	$1,748	$2,297	$2,843
17-20	$738	$858	$1,474	$2,167	$2,846	$3,532
21-24	$888	$1,005	$1,750	$2,575	$3,400	$4,230
25-28	$1,035	$1,164	$2,034	$2,986	$3,957	$4,912
29-32	$1,186	$1,311	$2,302	$3,402	$4,509	$5,612
Covers	$149	$164	$219	$275	$335	$393

International (includes Canada and Mexico))						
# of Pages	50	100	200	300	400	500
1-4	$306	$321	$467	$642	$811	$986
5-8	$387	$517	$816	$1,154	$1,498	$1,844
9-12	$574	$689	$1,157	$1,686	$2,190	$2,717
13-16	$754	$874	$1,506	$2,193	$2,883	$3,570
17-20	$710	$1,063	$1,852	$2,722	$3,572	$4,428
21-24	$1,124	$1,242	$2,195	$3,231	$4,267	$5,300
25-28	$1,320	$1,440	$2,541	$3,738	$4,957	$6,153
29-32	$1,498	$1,616	$2,888	$4,269	$5,649	$7028
Covers	$211	$224	$324	$444	$558	$672

Minimum order is 50 copies. For orders larger than 500 copies, please consult Cadmus Reprints at 800-407-9190.

Reprint Cover

Cover prices are listed above. The cover will include the publication title, article title, and author name in black.

Shipping

Shipping costs are included in the reprint prices. Domestic orders are shipped via FedEx Ground service. Foreign orders are shipped via a proof of delivery air service.

Multiple Shipments

Orders can be shipped to more than one location. Please be aware that it will cost $32 for each additional location.

Delivery

Your order will be shipped within 2 weeks of the journal print date. Allow extra time for delivery.

Tax Due

Residents of Virginia, Maryland, Pennsylvania, and the District of Columbia are required to add the appropriate sales tax to each reprint order. For orders shipped to Canada, please add 7% Canadian GST unless exemption is claimed.

Ordering

Reprint order forms and purchase order or prepayment is required to process your order. Please reference journal name and reprint number or manuscript number on any correspondence. You may use the reverse side of this form as a proforma invoice. Please return your order form and prepayment to:

Cadmus Reprints
P.O. Box 751903
Charlotte, NC 28275-1903

Note: Do not send express packages to this location, PO Box.
FEIN #:541274108

Please direct all inquiries to:

Rose A. Baynard
800-407-9190 (toll free number)
410-819-3966 (direct number)
410-820-9765 (FAX number)
baynardr@cadmus.com (e-mail)

Reprint Order Forms and purchase order or prepayments must be received 72 hours after receipt of form.